Study of Simulation Cell Size in Mean-Field Studies of Interacting Lattice Models

Yueguang Shi and Warren E. Pickett*

Department of Physics, University of California Davis, Davis CA 95616, USA.

Abstract. A lattice model of interacting fermions is studied with the principal aim of assessing the dependence of calculated mean-field ground states versus the $N \times N$ lattice size, with $N = 16$, 32, and 48. A two band model on the two-dimensional square lattice is simulated, with on-site energies and interaction parameters chosen to represent crystal field split orbitals in the moderately correlated regime. Nearest neighbor hopping leads to the well known van Hove singularities (vHs) of the square lattice. Anomalies in the inverse participation ratio of the eigenstates are found to be associated with the vHs, with their prevalence decreasing inversely with N. For the chosen model, inhomogeneous spin densities are always obtained for the small lattice size $N = 16$, with the degree of variation decreasing rapidly for most polarizations as N is increased. Various spin polarizations are treated, and one case in which spin density inhomogeneity persists for the largest lattice size is discussed and analyzed. Coupling of spin density inhomogeneities to charge density variation is minor but evident, and is primarily of intra-orbital origin.

PACS: 71.10.Fd, 71.15.Dx, 75.30.Fv, 75.10.Lp

Key words: Lattice Hamiltonian, mean field, lattice size, moderate interactions.

1 Introduction

The study of inhomogeneous phases in correlated electron systems has long been an area of active investigation, with the spin density wave in chromium providing an early example [1]. Activity increased strongly after the discover of charge density stripes in hole-doped $La_{1.6-x}Nd_{0.4}Sr_xCuO_4$ with $x = 0.12$ [2], in hole-doped manganites $La_{1-x}Ca_xMnO_3$ [3] and $La_{0.5}Sr_{1.5}MnO_4$ [4], and also hole-doped nickelates $La_2NiO_{4.125}$ [5] and $La_{1.67}Sr_{0.33}NiO_4$ [6]. The classic inhomogeneities, charge density waves (CDW) and spin density waves (SDW) have conventionally been tied to Fermi surface nesting [1], though

*Corresponding author. *Email addresses:* `wepickett@ucdavis.edu` (W. E. Pickett), `ygshi@ucdavis.edu` (Y. Shi)

a close connection to CDWs to nesting has been questioned [7]. Density wave states have by definition a specific wavelength λ and direction, hence a specific wavevector $\vec{q}$, $q = |\vec{q}| = 2\pi/\lambda$, related to Fermi surface calipers.

Theoretical study of these inhomogeneities began in earnest in response to reported inhomogeneities in cuprates, newly discovered to be high temperature superconductors when hole-doped. These investigations focused on the square lattice Hubbard model doped away from the antiferromagnetic ordered state at half filling and treated in a mean field (Hartree-Fock) manner. Su obtained spin polaron states [8] building on the spin-bag mechanism of electron pairing that had been introduced by Schrieffer, Wen, and Zhang [9]. Machida used an approach somewhat more from the itinerant side and obtained a soliton lattice spin structure and striped charged domain walls [10]. Zaanen and Gunnarsson extended such studies to a two-band model, finding charged magnetic domain walls (charge and associated spin stripes) or a ring of such a wall, depending on the periodicity enforced by 9×10 versus 10×10 periodic lattices [11]. This work may have been the first to indicate the effect of lattice (simulation cell) size and commensurability on the resulting ground states that are obtained. More on such studies, and the methods that were developed, will be discussed in Section 2.

Since this early work, numerous related papers have appeared (some of the early papers have accumulated hundreds of citations), with much of the effort turning to dynamical inhomogeneities or more varied spatial inhomogeneities, and how they impact the properties of strongly correlated electron systems. Nevertheless studies of static charge and spin stripe ground states have persisted, with extensions to more nuanced models aimed at modeling specific classes of materials, viz. manganites versus cuprates versus iron pnictides. Dagotto and coworkers have reported studies on a two orbital model adapted to model the d_{xz}, d_{yz} orbitals of iron pnictides, finding stripes for periodic Hamiltonians and disturbed stripes for cases with quenched-in disorder, such as by Co doping [12, 13]. A recent direction has been to move beyond mean field approaches for multi-orbital models by extending quantum Monte Carlo methods to study such charge and stripe correlations [14, 15]. Meanwhile, experimental investigations have become more detailed, by mapping symmetries of inhomogeneous phases using, for example, advanced spectroscopic imaging [16, 17] in addition to diffraction.

Most previous studies have concentrated on the strongly correlated regime. When interaction effects are strong, effects of the underlying mean field Fermi surface assume less importance; conversely moderately correlated systems may retain instabilities connected to the Fermi surface. In the latter scenario, reasonable sampling of the Fermi surface requires larger simulation cells. This is the feature we address in this paper: for a moderately correlated two-orbital (two-band) lattice model, how does the calculated ground state depend on the lattice size in the simulation.

The organization of the manuscript is as follows. In Section 2 the two band model and methods of treatment are presented. Section 3 presents some baseline results for the density of states (DOS) and the inverse participation ratio of the single particle eigenstates, related to lattice size $N \times N$ with $N = 16, 32$, and 48. Results for interacting particles

relating to lattice size dependence, orbital differentiation, and dependence on spin polarization are presented in Section 4. Section 5 provides a brief discussion and summary.

2   Methods

2.1   The multi-orbital model

We deal with a two orbital basis, with particles hopping on a square lattice and interacting via repulsive on-site interactions $U_{\alpha\beta}$. The Hamiltonian is

$$H = \sum_{i\alpha\sigma} \varepsilon_\alpha n_{i\alpha\sigma} + \sum_{<ij>\sigma} \sum_{\alpha\beta} c^\dagger_{i\alpha\sigma} t_{\alpha\beta} c_{j\beta\sigma} + \frac{1}{2} \sum_{i\sigma} \sum_{\alpha\beta} n_{i\alpha\sigma} U_{\alpha\beta} n_{i\beta\sigma}. \tag{2.1}$$

Here $t_{\alpha\beta}$ is the hopping amplitude between orbital α at site i and orbital β on a neighboring site, and $\langle ij \rangle$ indicates the sum is over nearest neighbors in each direction. ε_α is the on-site energy of each orbital, and σ indicates the spin projection up and down. The operator $c^\dagger_{i\alpha\sigma}$ creates a particle of spin σ and orbital α on site i, and $n_{i\alpha\sigma} = c^\dagger_{i\alpha\sigma} c_{i\alpha\sigma}$ is the corresponding number operator.

Multi orbital models of this sort have occasionally been addressed with beyond mean field methods, but the doubling of basis size further restricts the size of simulation supercell that can be handled numerically. A primary purpose of the current work is to study the effect of supercell (also referred to as lattice, with periodic boundary conditions) size on the resulting ground states. Using quantum Monte Carlo methods, even single orbital models usually don't explore lattice sizes larger than around 12×12.

We will obtain mean field solutions to this model and demonstrate that even with two orbitals one can reasonably simulate up to 48×48 lattices in the moderately correlated regime that we study. For the two orbital model the basis size is $2N^2 = 4608$ for $N = 48$. Moreover, with several parameters in the model as well as the filling fraction (mean number of particles per orbital) and the spin polarization, it is necessary to restrict ourselves to a particular regime of hopping and interactions.

While inhomogeneous states (charge and spin stripes, for example) have been of interest for some time in the strongly correlated regime (viz. cuprates and manganites), the question has resurfaced due to observation of inhomogeneous phases in less highly correlated metals, especially the iron pnictides and chalcogenides that provide the platform for high temperature superconductivity in the range of $T_c \sim 60K$. For this reason we choose model parameters that mimic t_{2g} and e_g orbitals, which generically have similar bandwidths (hopping amplitudes) and intra-atomic repulsion but a crystal field splitting of 1-3 eV, thus on-site energies differing by this amount.

The parameters we choose, for orbitals 1 and 2, are on-site energies $\varepsilon_1 = 1$, $\varepsilon_2 = -1$, nearest neighbor hopping amplitudes $t_{1,1} = 1$, $t_{2,2} = -1$, and on-site repulsions $U_{1,1} = 2 = U_{2,2}$, $U_{1,2} = U_{2,1} = 0.5$. In a multi orbital system without a special selection of parameters, band filling is not a crucial degree of freedom. We choose half-filling (one electron

per orbital, on average) as most relevant to stoichiometric materials, and the crystal field splitting keeps the noninteracting Fermi level away from van Hove singularities except accidentally at certain polarizations. The two parameters we vary are the spin polarization P and the lattice size, comparing N^2 lattice sizes with $N = 16, 32$, and 48. The polarization is given by

$$P = \frac{n_{up} - n_{down}}{n_{up} + n_{down}} \tag{2.2}$$

in terms of the number of up n_{up} and down n_{dn} particles. The mean spin is $\langle S \rangle = 2P$.

2.2   Method of solution

A few approaches to treating multiorbital models in mean field have been suggested and used. Hess and Serene pioneered a method adjusted to results of a many body solution of multi-orbital models [18]. They devised a density functional theory (DFT) inspired approach, fitting a polynomial expansion of the exchange-correlation functional to fluctuation-exchange approximation solutions of the interacting Hamiltonian. We have used their method, since our model corresponds to moderately correlated electrons where such a DFT-inspired method may be reasonable. We note that a more direct lattice DFT for the single band Hubbard model has been proposed and studied by Lopez-Sandoval and Pastor [19].

Luo *et al.* have studied a two orbital model of iron pnictides in a similar regime of interaction, applying the Hartree-Fock approximation conventionally applied in single orbital models [12]. Their Supplemental Material can be consulted for the type of coupled equations that must be solved iteratively to self-consistency. They obtained solutions for $N = 16$ lattices that contain charge stripes along the axes. Considering the difference in model parameters and methods of solution, no useful comparison with their work can be made. As mentioned above, there are continuing studies to treat multi-orbital models with non-mean-field (Monte Carlo, exact diagonalization). For example, Kung *et al.* have studied a three orbital model of cuprates [14], but proliferation of states and the fermion sign problem limited them to modest sized clusters.

2.3   Convergence

For convergence we have been satisfied with linear mixing of 15% of output with 85% of input for the new input, 'input' being the site, orbital, and spin dependent densities. No doubt improvements can be made over linear mixing [20], and should be done in future studies especially for more strongly correlated models where convergence is more of a challenge. Our criterion for convergence was that the root mean square difference between input and output orbital densities over the lattice is less than 10^{-5} for each spin. For each choice of lattice size and spin polarization, several runs were used with a different choice of random initial wave functions. Although there are clear visual differences in the resulting charge and spin densities which are to be expected, the character of the

inhomogeneities is similar for each run and the differences in total energies are negligibly small. Examples will be provided in the Supplemental Material. In preliminary studies using parameters representing stronger correlations (as for a doped Mott insulator or a Kondo metal), sometimes 2-4 different classes of states would be reached, which would be differentiated by small but distinctive differences in total energy. We found that we obtained only one type of solution (differences only in insignificant detail) in all cases except one, which is discussed in Section 4.

3 Base line issues

3.1 Density of states

Since the emphasis in this paper is on the effect of lattice size, one first item to survey is the degree to which the desired (infinite) system is modeled and sampled by finite lattices. The densities of states before interaction are displayed in Fig. 1 for lattice sizes $N = 16$, 32, and 48. The infinite lattice result for a single orbital is well known: a bandwidth of $W = 8t$ with step discontinuities at the band edges, and a divergent singularity at the band center arising from the van Hove singularity at the center of the band, at the zone boundary X points for the infinite lattice. Fig. 1 shows the lattice DOS for the two
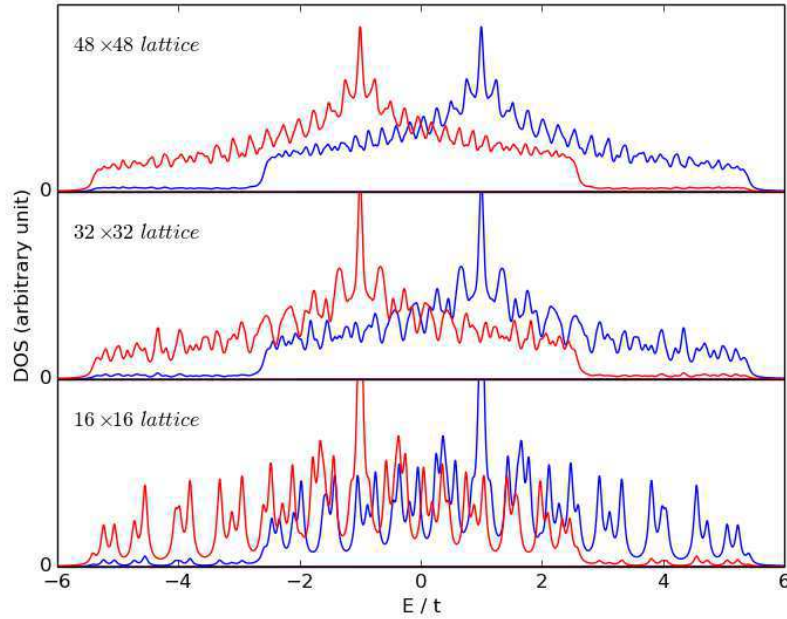

Figure 1: The non-interacting density of states for the $N = 16,32$, and 48 simulations cells, as labeled. The lower (red) and upper (blue) bands are uncoupled. The progression illustrates the relative sampling of states in energy for the three cases.

bands, which are $N \times N$ δ-functions for each band that have been broadened by $\gamma = 0.05$ in units of $t = 1$ (0.6% of the bandwidth $W = 8.0$). As is well recognized, the $N = 16$ lattice gives a relatively crude representation of the exact DOS, with rather little definition that is evident in the exact DOS. The full square symmetry leads to $(N/2)[(N/2)-1]/2$ distinct eigenvalues, which is 28 for $N = 16$, 120 for $N = 32$, and 276 for $N = 48$. For $N = 16$ the DOS peak in the vHs region is represented as a single isolated peak above a ragged background. For $N = 48$ the infinite lattice behavior is becoming evident. Of course with interactions included and inhomogeneous states arising, all $2N^2$ eigenvalues will be distinct.

Doubling the lattice to $N = 32$ (four times as many eigenvalues) evidences the exact structure fairly well. The (step function) band edges are not very well defined, but the logarithmic singularity can begin to be imagined. Proceeding to $N = 48$, nine times as many eigenvalues as for $N = 16$, the sampling noise in the DOS is beginning to become regular around what will emerge in the thermodynamic limit. In particular, the vHs peak height is proceeding toward having a realistic weight relative to other states, whereas for the smaller lattices the weight was much more dependent on the density of sampled states near the vHs. The DOS is reproduced well enough that any further influence of the vHs DOS singularities might require additional algorithms.

3.2 Inverse participation ratio

A point of interest is the degree of itinerancy of the eigenstates when correlation effects lead to inhomogeneous states, as we will find and discuss later. The itinerancy versus inhomogeneity (localization) of eigenstates is conventionally measured by the inverse participation ratio (IPR), defined by

$$IPR = \sum_{ij\alpha} \psi_{ij\alpha}^4 / \sum_{ij\alpha} \psi_j^2, \tag{3.1}$$

where the sum is over all $2N^2$ ($i, j = 1$ to N, orbitals $\alpha = 1, 2$) components of the state, however the denominator is the normalization to unity. With this definition the ideally itinerant (uniform) state with equal amplitudes on all sites and each orbital will have $IPR_{min} = 1/(2N^2)$ while the absolutely localized state in a single orbital has IPR=1 independent of lattice size. If certain sites have amplitudes ψ_j larger than average, they contribute more to the sum and increase the IPR above IPR_{min}. The absolute magnitude of the IPR may carry some interest, but it is variations or deviations from "typical" or background that are of most interest. We have verified that in the absence of interaction, the IPRs are all equal – all noninteracting states are uniform – so there is no interesting variation imposed by the periodic lattice.

The calculated IPRs for $P = 1/4$ and the $N = 16, 32$, and 48 lattices are shown in Fig. 2. In all cases the spin down values are not appreciably different from those of spin up, and we have found that there is no interesting dependence on P. There is a smooth background of IPR(E) that is minimum near the band edges and roughly a factor of two
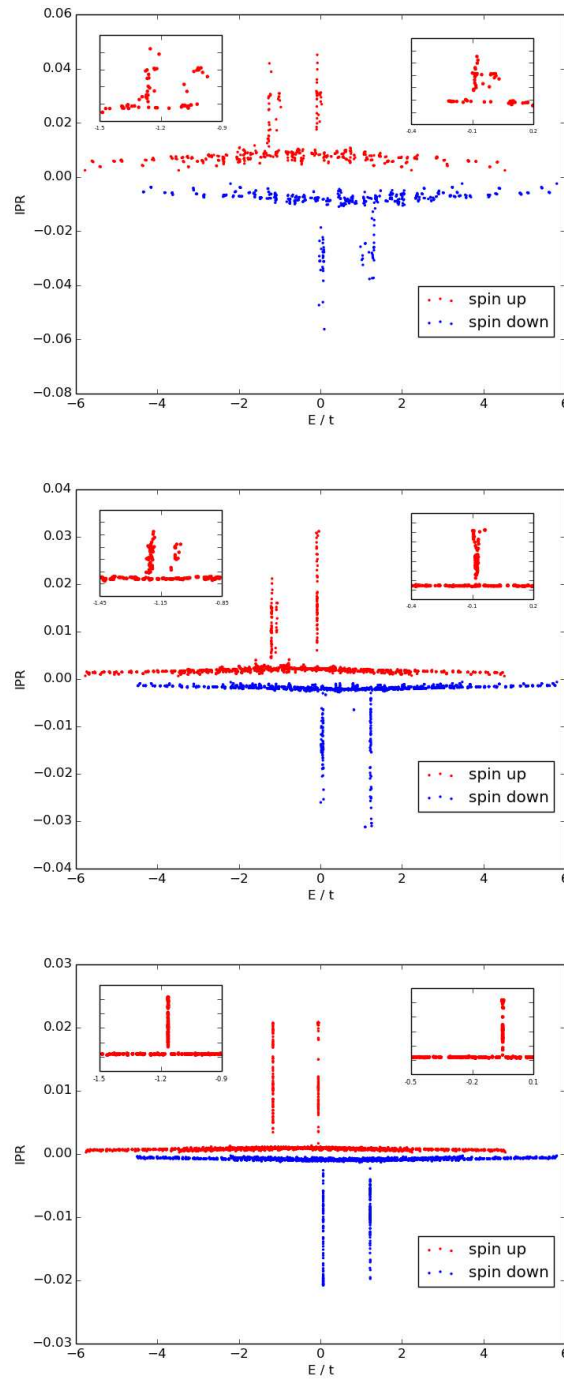
Figure 2: The inverse participation ratio for all eigenstates for polarization $P=1/4$. Panels from top to bottom: $N=16, 32, 48$. Values for spin down are plotted as negative values.

larger around band center: the eigenstates are less homogeneously distributed where, roughly speaking, there are most closely spaced states. Note that the IPR can increase due to variation of amplitude from site to site (the common reason) but also due to increase in orbital polarization, that is, imbalance in orbital amplitudes on the same site. Since the "background" is continuous from the single band regions at top and bottom, to the two-band region in the middle, orbital polarization effects must be minor for our choice of model.

The distinctive feature of the IPR distribution is the concentration of large values, 10-15 times larger than for the other energies, at the vHs of both bands. This feature is persistent across all polarizations that we have studied, with one exception that will be discussed below. The insets in Fig. 2 indicate that these peaks can contain a little structure for smaller values of N. For $N=16$, the large values of IPR at the vHs consist of up to two separate classes separated by an energy as large as 0.1. For larger N there is only a single "peak" at each vHs. For $N=48$ the separation of such peaks at the vHs from the smooth background becomes clear. Counting the large IPRs, within statistical scatter the number of large values is $2N$, compared to the number of eigenvalues $2N^2$. For example, for the values shown in Fig. 2 the number is 35, 63, and 93 for $N=16$, 32, and 48, respectively.

The scaling of the number of large values of IPR can be analyzed in terms of effective sampling of the zone that depends on lattice size, but might also depend on the parameters of the model. A non-interacting vHs for the square lattice is distinguished by a saddle energy surface centered at the point of vanishing velocity, with a divergent $N(E)$ as the vHs is approached. Using a finite simulation lattice amounts to sampling the BZ with N^2 evenly spaced points, one of which lies on each of the two partners of a given vHs [at $(\pi,0)$ and $(0,\pi)$]. Each vHs point is surrounded by eight neighboring k-points, four along the diagonal with the identical vHs energy, and four along the axes with energies that differ to second order in their distance from the vHs point. The $2N$ states with large IPR may contribute spurious contributions to the results, but these contributions scale as $2N/2N^2 = 1/N$, vanishing (somewhat slowly) with increasing lattice size.

4   The interacting system

4.1   Lattice size dependence

As mentioned earlier, a primary aim of this work is to assess the lattice size dependence of inhomogeneities that arise. We remind that our self-consistent procedure begins from random wave function components, subject to normalization. With interaction included, some amount of inhomogeneity is always found, but often it is small enough to be negligible (possibly an artifact of finite lattice size, or unphysical and unimportant contributions from vHs). We have however verified that the inhomogeneities do not decrease when we choose a more stringent convergence criterion, changing the convergence criterion from 10^{-5} to 10^{-7} for the root mean square difference between output and input orbital charge and spin densities. Because of the random starting wave function coeffi-

cients, the exact same inhomogeneity will never be reproduced in a parallel run. There is the small probability of obtaining symmetry related states of course, but in practice we observe recognizable visual differences in the states that are obtained. For our choice of parameters, however, the *degree of inhomogeneity* is always similar if there is significant inhomogeneity, and the variation in total energies of the self-consistently obtained states is quite small. Thus the specific results that we display and discuss are representative of a general class of similar "ground states" for a given polarization. Further clarification is provided in the Supplemental Material.

In Fig. 3 the real space variation, for $P=1/4$, of both charge and spin densities is displayed, first for each orbital, then for the total (the sum over orbitals). The chosen lattice sizes result in the areal pixel density increasing by almost an order of magnitude from $N=16$ to $N=48$, and the difference in resolution is immediately evident. One could present results in another fashion, by comparing the (say) $N=48$ displays with a 3×3 array of identical $N=16$ lattices, in which the "resolution" and actual real space lattice spacings would be the same. We have chosen to display so the basic $N\times N$ lattice is the same display size for all N.

The most important item on the array plots to notice is the variation of the total charge and spin density, as reflected in the accompanying color bar. In our studies we have kept the average charge/site at two, and fixed spin polarization P. With two orbitals, the mean spin per site $\langle S\rangle=2P$. For $P=1/4$ and for $N=16$, 32, and 48 respectively, the range of site charges are 1.985-2.025, 1.995-2.035, 1.999-2.002 while the ranges for spins are 0.1-0.7, 0.3-0.6, 0.49-0.51. The range need not be symmetric around the value of total charge (2.000) or spin (0.500) because the inhomogeneities are not symmetric around these values, but they are roughly symmetric in practice. The "range" of variation is often determined by a few relatively large or small values (local moments) compared to those of most of the sites.

For our moderately correlated choice of model parameters, large variations in charge are not anticipated, and progression of the variation with lattice size, from 0.04 to 0.003 with increasing lattice size, signals negligible charge variation in the large N limit. Our results do indicate that lattices of modest size can encourage some small and unphysical charge variation. Notice that these small (but still unphysically large) inhomogeneities organize themselves into patterns: diagonal stripes for $N=16$, ribbons of diagonal stripes for $N=32$, and finally the very small variations for $N=48$ form superstructures with a diagonal motif. This appearance of charge inhomogeneity that vanishes for large lattice sizes results from a combination of coupling to spin inhomogeneity in concert with quantum confinement (or forced commensuration with) the finite lattice size.

The range of spin inhomogeneity is more interesting. For the $N=16$ lattice there are isolated sites with small moment ~ 0.1 neighboring sites with moments of 0.4 and 0.7, arrayed more or less on a square superlattice comprised of every third site. This motif seems to be preferred, but since 3 is incommensurate with $N=16$, there is a disruption of this pattern along one diagonal to accommodate to the lattice size. For $N=48$, the spin inhomogeneity has become so small that it will disappear in the large N limit. As was
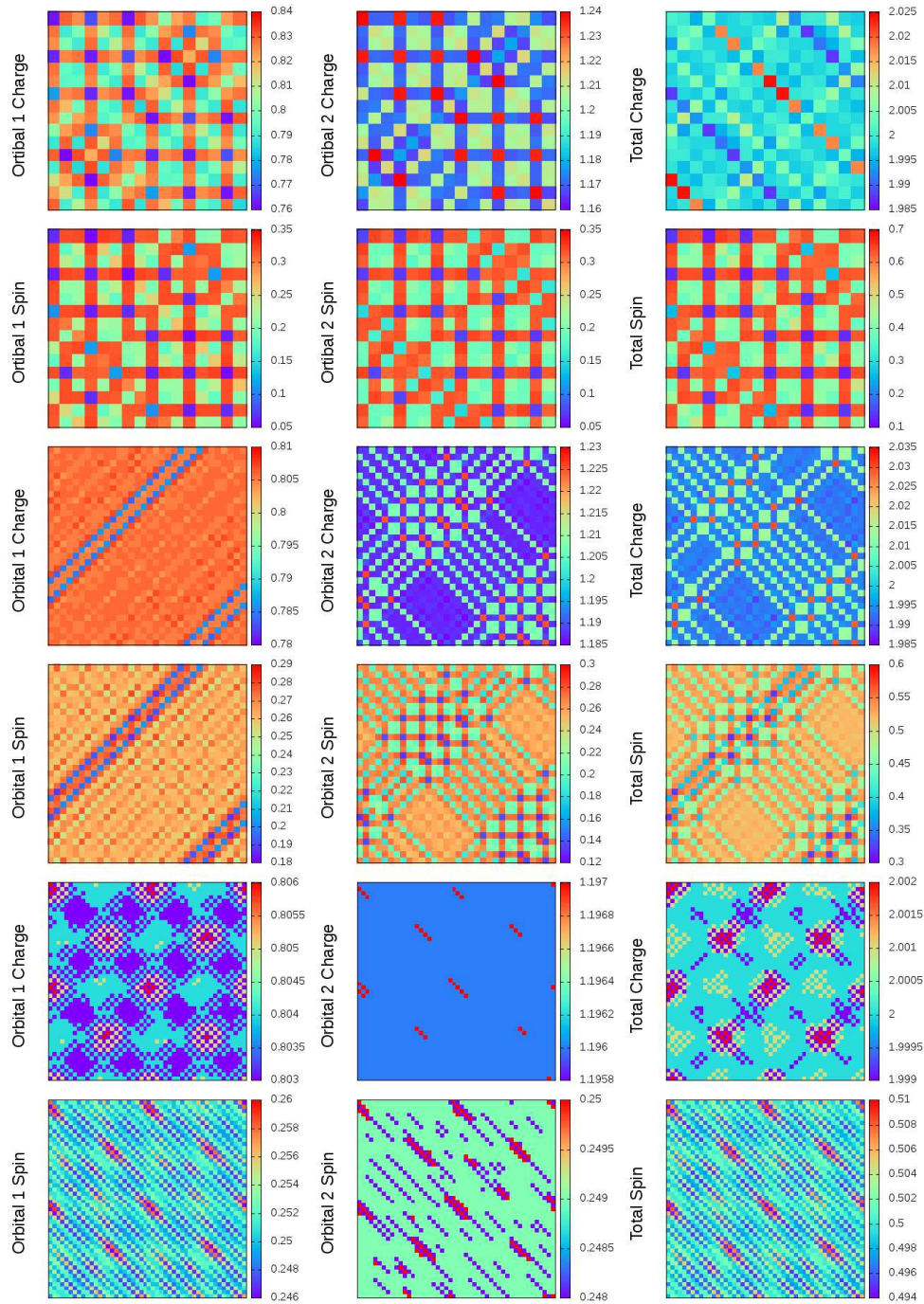
Figure 3: Charge and spin density arrays for polarization $P = 1/4$. The top six panels are for $N = 16$, charge arrays above spin arrays, and from left to right progressing from orbital 1 to orbital 2 to the total (their sum). The center six panels are for $N = 32$, the lower six panels are for $N = 48$. Note the magnitude of variation (color bar); the variations are vanishing as lattice size increases.

the case for the charge variation, the spin inhomogeneity typically vanishes in a patterned manner consistent with the lattice size.

4.2 Differences between the two orbitals

Even a cursory examination of the density array color plots reveals that

1. the inhomogeneities of the two orbitals are often quite different;

2. the inhomogeneities of charge and spin within each orbital are related.

Our conclusion, already mentioned above, is that our moderately interacting system shows no CDW phases nor any significantly inhomogeneous charge density. However, significant spin inhomogeneity does sometimes appear, and that spin variation clearly couples to the charge: the patterns of variation have much similarity although the charge variation for the largest lattice size never seems significant.

The charge inhomogeneity for $N = 16$ decreases with lattice size, and it is important to note that it does not decrease with stricter convergence criteria, as confirmed by tightening the convergence criteria of rms deviation between output and input from 10^{-5} to 10^{-7}. Spin density (and charge density) inhomogeneities on orbital 1 can be different from those on orbital 2, but each correlates with its own spin variation, reflecting intraorbital spin-charge coupling.

With the total charge at an average of two per site, the system can be characterized as half filled. The usual connotations of this designation do not apply here, first because the system is always metallic, and second because of the "crystal field splitting" the orbital occupations are different, and specifically well away from unity. Apart from the patterns of the slight variation, the only changes that occur when we change polarization is the contribution from each orbital. When P approaches unity (15/16 was simulated), the charge in orbital 2 is larger by 0.1. When P decreases, this value increases. When $P \rightarrow 0$ ($P = 1/16$ was studied), charge in orbital 2 is larger by 0.45.

4.3 Polarization dependence versus lattice size

There are three main types of patterns that appear for the smaller lattice sizes: stripes, ordered clusters, and chessboard, none of which are perfectly ordered. Stripe patterns are primarily diagonal, usually observed as multiple stripes along one diagonal direction. Occasionally stripes along an axis appear. When $P = 1/4$, different wide stripes are observed, some also have stripes that cross from both diagonal directions. Cluster patterns are areas of different density occurring in an ordered manner, while chessboard is an arrangement where for every pixel, neighboring pixels have a different value (color).

A trend, after analyzing inhomogeneities at several polarizations, seems to be that stripes are somewhat more common at larger polarization, clusters and chessboard are more common at smaller polarization. Since this model is in the moderate correlation regime, Fermi surface effects may arise (the underlying Fermi surfaces are even discussed

for strongly correlated system where real space pictures become more useful). Looking at Fig. 1 and recalling the particle-hole symmetry, at $P=0$ the two Fermi surfaces are identical but with one centered at Γ and the other at the zone corner M. Polarization increases (decreases) the number of up (respectively, down) spins, *i.e.* it raises E_F for up spins and lowers E_F for down spins by the same amount. For the up spins, the lower band Fermi surface will decrease in size, the upper band Fermi surface will decrease in size. For $P=1/4$ the larger Fermi surface is approaching diamond-shaped "half-filled" one of the single band tight binding model, with its associated (π,π) nesting and van Hove singularities at $(\pi,0)$. A nesting argument would explain alternating stripes along the diagonals. In Fig. 3 ($P=1/4$), the $N=16$ case is not easy to categorize objectively. For $N=32$ well developed stripes do arise. However, for $N=48$ the homogeneity has nearly disappeared (note the scales of variation). Thus nesting does not account for the $P=1/4$ result, but it may be a factor in the trends with increasing P.

4.4　Ground state of the $P=0$ case

The unpolarized ground state stands out from most of those with polarization in two striking ways. First, large spin variation persists to the largest lattice size. The only other example of this was for $P=3/16$, with a few results presented in the Supplementary Material. Second, two different types of states are obtained. Three examples of the *stripe* state are displayed in Fig. 4, and three examples of the *pattern* state are provided in Fig. 5. Both have moments, positive and negative, of magnitude 0.3-0.4. Also, both display very small charge (nearly negligible) variations that are associated with the large spin variations. We emphasize that each state, and only these states, were obtained in several simulations starting from random wave functions.

　　The *stripe* state (Fig. 4) consists of six columns along an axis, with a 'dead' region of a width of roughly two stripes. The stripe columns, 3-4 sites in width, have an internal structure of large moments anti-aligned on neighboring sites. The contributions from each orbital are similar. The very small charge variations follow that of the spins.

　　The *pattern* state (Fig. 5) is somewhat more intricate. There are 2-3 stripes along an axis, spaced as in the *stripe* pattern but varying somewhat in intensity along the stripe. The rest of the lattice contains a rather regular array of $\sim 3\times 3$ clusters of spins, again anti aligned within a cluster as in the stripes. These clusters are separated by ~ 3 dead (spineless) sites. Again, the contributions from each orbital are similar. The very small charge variation appears different but actually follows the spin pattern except with less abrupt variation.

　　The occurrence of two, or sometimes more, metastable states is well known in such mean field simulations. The energy landscape can contain several local energy minima with small differences, and the iteration procedure finds one or another depending on starting point and type of iteration algorithm. We have observed (for model parameters different from those of the present study) that local minima are more prevalent as the interaction strength is increased relative to the bandwidth. One distinction of the $P=0$
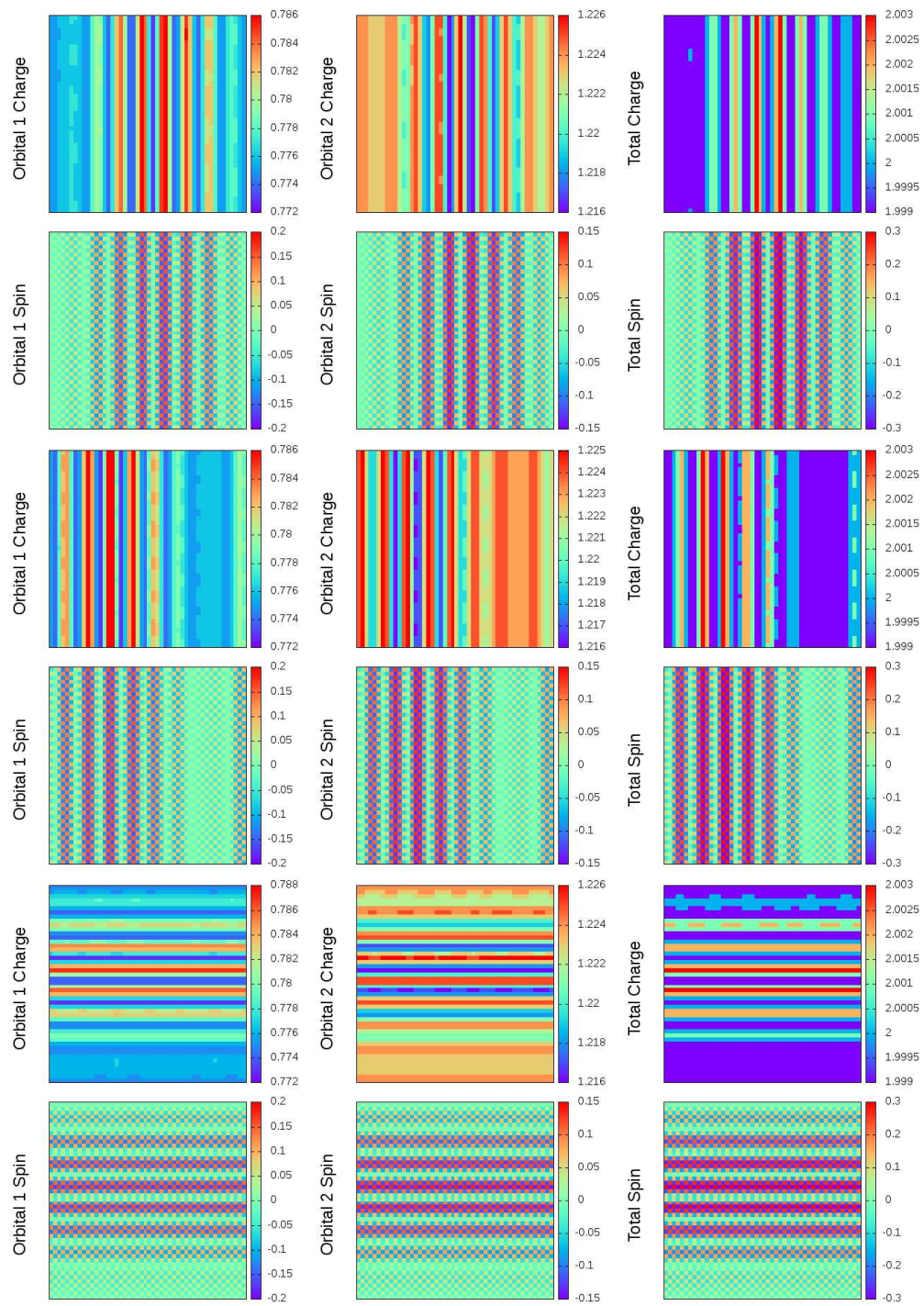
Figure 4: Three examples of the *stripe* type of ground state for polarization $P=0$. Each example consists of six panels, three above for charge and three below for spin. The color bar provides the amplitudes.
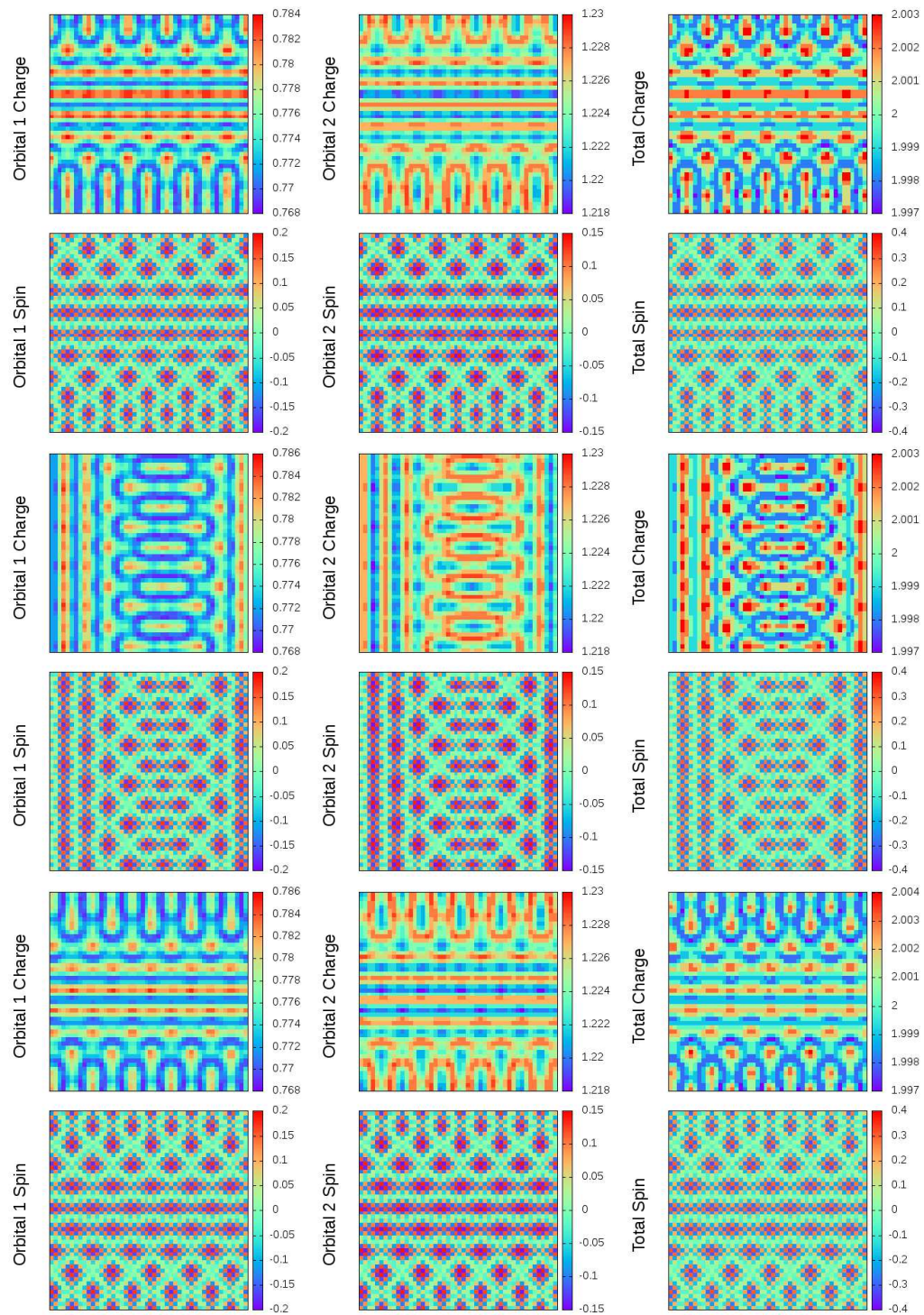
Figure 5: Three examples of the *pattern* type of ground state for polarization $P=0$, presented as done in Fig. 4.

system is that the non-interacting Fermi surfaces, which are closed lines surrounding the zone corner, coincide. This is a consequence of the particle-hole symmetry of our choice of parameters and half-filling. There is however no significant nesting of the surfaces.

The difference for $P=0$ extends to the IPR, both the character and (in)dependence on lattice size. Fig. 6 can be contrasted with Fig. 2 for $P=1/4$. Versus lattice size, the distribution does not change character, only becoming better defined with increasing lattice size. However, the distribution differs from that for the polarized systems. The peaks occur in the regions of the vHs but with substantial extension in energy. The IPR values are somewhat larger as well, as expected for more inhomogeneous states. However, the IPRs of the *stripe* and *pattern* states are very similar, as are their DOSs.

5   Discussion and summary

In this study we have focused on the effect of lattice simulation size, using $N \times N$ sites with $N = 16, 32$, and 48, on a lattice model of interacting electrons treated in mean field approximation. The model has two orbitals in the unit cell with different on-site energies (hence different band centers), with both hopping and on-site Coulomb repulsions between the same and also opposite orbitals. Unlike the predominance of previous studies, we have focused on the moderately correlated regime where Fermi surface, or other long wavelength processes may be in play, thus where lattice size should be more of a factor.

Due to the number of parameters in the model it was necessary to choose one set and analyze the effect of lattice size as spin polarization was varied. The parameters that were chosen represent a moderately correlated two-orbital system such as have been used for Fe-based pnictides and chalcogenides, where emergence of charge or spin inhomogeneities may occur but are not certain to do so. This regime is likely to be more sensitive to lattice size in the simulation than for systems in the strongly correlated regime where the physics is more local in nature.

A strong trend that emerged for most polarizations is that spin inhomogeneities are present for $N=16$, they decrease in amplitude for $N=32$, and become so small for $N=48$ that the expectation is that the ground state is homogeneous in the large-N limit. When the spin inhomogeneities are seen, a common motif is diagonal stripe-like correlations in the square lattice, with occasionally stripes along the axis or clusters being observed. As mentioned, these inhomogeneities usually vanish as the lattice size increases, with only $P=0$ and $P=3/16$ showing persistent spin density variation. Inhomogeneities of charge accompany those of the spin and are parasitic off the spin polarization, but they are always very small so there is no true charge instability in our model.

The aforementioned behavior holds for the spin polarizations up to the large value of $P=1/2$ that we simulated. The different behavior found in the non-polarized case was discussed is some detail. This system displayed a roughly random distribution of local moments of varying sizes, with the same character for all three lattice sizes. Charge density variation was still minor, i.e. parasitic off the spin-dependent interaction and
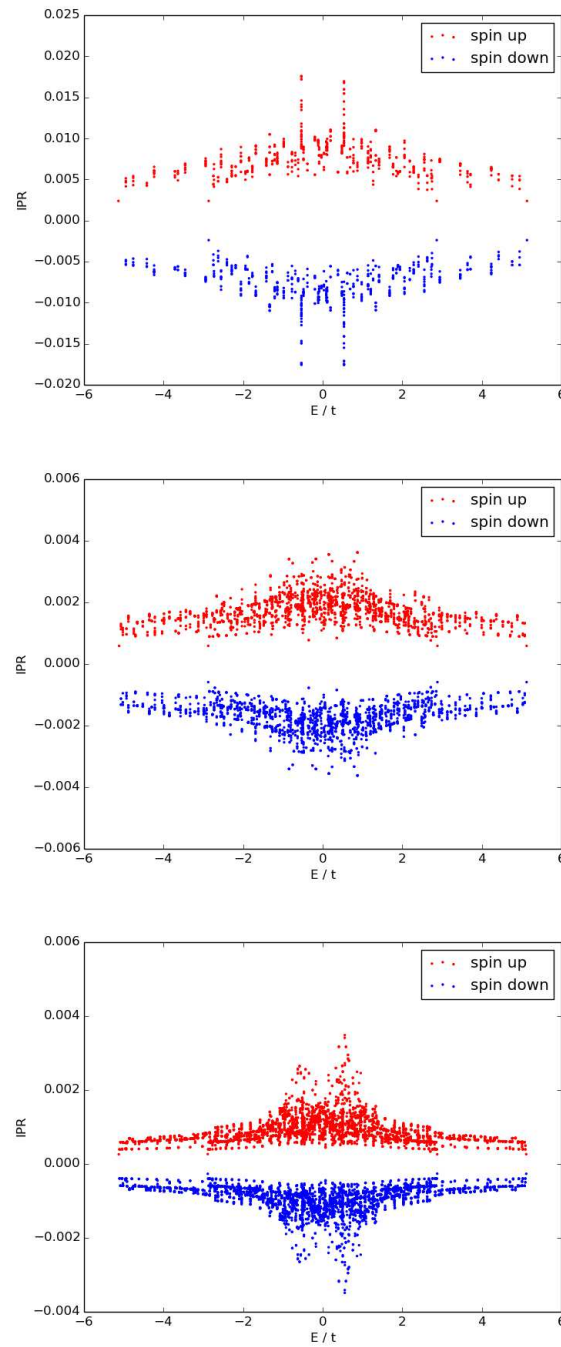
Figure 6: The inverse participation ratio for all eigenstates for the unpolarized case $P = 0$. Panels from top to bottom: $N = 16, 32, 48$. Values for spin down are plotted as negative values. Up and down results are effectively identical in spite of starting from distinct random wave functions. Up and down IPRs are effectively identical, in spite of starting from random wave functions in every run.

becoming insignificant with large lattice size. It should be emphasized that the same character of ground state was obtained for several calculations beginning from random wave functions; the result appears to be robust. We have not identified any reason for the different behavior for $P=0$ and $P=3/16$ relative to the other polarizations. No Fermi surface effect is implicated, in fact for nearly all cases the spin variation vanishes as the Fermi surfaces is sampled more carefully ($N=48$).

The inverse participation ratio was monitored in the simulations, as a quantity that measures the inhomogeneity of individual wave functions. For the polarized cases, the IPR was smooth with energy of the state except for elevated values (by a factor of 3-5) in a very narrow range precisely at the van Hove singularities. The fraction of states with larger values of the IPR is proportional to $1/N$, hence there we have no reason to believe that vHs have undue influence on the ground state in the thermodynamic limit, note that they coincide with the Fermi level only for isolated values of polarization. Again, the $P=0$ case is different: large values of IPR again occur centered at vHs, but the range in energy with enlarged IPR is increased to $\sim 10\%$ of the bandwidth.

We emphasize that specific behaviors and trends we have pointed out may be representative only of moderately correlated, few bands models. Details will surely be dependent even on the choice of model parameters. General expectations are that models in the strongly correlated regime will be dominated by more local behavior. As such, their behavior should be less dependent on lattice size, but organized structures such as stripes or clusters can still emerge. Conversely, moving to the more weakly correlated regime, Fermi surface effects may become more important. If so, inhomogeneous structures tied to the Fermi surface will be lattice size dependent as the Fermi surface becomes more closely sampled for larger lattices. These speculations remain to be confirmed, of course, since very few studies have been done with large lattices.

Acknowledgments

References

[1] L. M. Corliss, J. M. Hastings, and R. J. Weiss, Antiphase Antiferromagnetic Structure of Chromium, Phys. Rev. Lett. **3** (1959) 211.
[2] J. M. Tranquada, B. J. Sternlieb, J. D. Axe, Y. Nakamura, and S. Uchida, Evidence for stripe correlations of spins and holes in copper oxide superconductors, Nature **375** (1995) 561.

[3] A. P. Ramirez, P. Schiffer, S-W. Cheong, C. H. Chen, W. Bao, T. T. M. Palstra, P. L. Gammel, D. J. Bishop, and B. Zegarski, Thermodynamic and Electron Diffraction Signatures of Charge and Spin Ordering in $La_{1-x}Ca_xMnO_3$, Phys. Rev. Lett. **76** (1996) 3188.

[4] B. J. Sternlieb, J. P. Hill, U.C. Wildgruber, G. M. Luke, B. Nachumi, Y. Moritomo, and Y. Tokura, Charge and magnetic order in $La_{0.5}Sr_{1.5}MnO_4$, Phys. Rev. Lett. **76** (1996) 2169.

[5] J. M. Tranquada, D. J. Buttrey, V. Sachan, and J. E. Lorenzo, Simultaneous Ordering of Holes and Spins in $La_2NiO_{4.125}$, Phys. Rev. Lett. **73** (1994) 1003.

[6] K. Yamamoto, T. Katsufuji, T. Tanabe, and Y. Tokura, Raman Scattering of the Charge-Spin Stripes in $La_{1.67}Sr_{0.33}NiO_4$, Phys. Rev. Lett. **80** (1998) 1493.

[7] M. D. Johannes, I. I. Mazin, and C. A. Howells, Fermi-surface nesting and the origin of the charge-density wave in $NbSe_2$, Phys. Rev. B **73** (2006) 205102.

[8] W. P. Su, Spin polarons in the two-dimensional Hubbard model: A numerical study, Phys. Rev. B **37** (1998) 9904(R).

[9] J. R. Schrieffer, X.-G. Wen, and S.-C. Zhang, Spin-bag mechanism of high-temperature superconductivity, Phys. Rev. Lett. **60** (1988) 944.

[10] K. Machida, Magnetism in La_2CuO_4 based compounds, Physica C **158** (1989) 192.

[11] J. Zaanen and O. Gunnarsson, Charged magnetic domain lines and the magnetism of high-T_c oxides, Phys. Rev. B **40** (1989) 7391.

[12] Q. Luo, D.-X. Yao, A. Moreo, and E. Dagotto, Charge stripes in the two-orbital Hubbard model for iron pnictides, Phys. Rev. B **83** (2011) 174513.

[13] E. Dagotto, Colloquium: the unexpected properties of alkali metal iron selenide superconductors, Rev. Mod. Phys. **85** (2013) 849.

[14] Y. F. Kung, C.-C. Chen, B. Moritz, S. Johnston, B. Thomale, and T. P. Devereaux, Numerical exploration of spontaneous broken symmetries in multi-orbital Hubbard models, Phys. Rev. B **90** (2014) 224507.

[15] E. W. Huang, C. B. Mendl, S. Liu, S. Johnston, H.-C. Jiang, B. Moritz, and T. P. Devereaux, Numerical evidence of fluctuating stripes in the normal state of high-T_c cuprate superconductors, Science **358** (2017) 1161.

[16] R. Comin, R. Sutarto, F. He, E. H. da Silva Neto, L. Chauviere, A. Frao, R. Liang, W. N. Hardy, D. A. Bonn, Y. Yoshida, H. Eisaki, A. J. Achkar, D. G. Hawthorn, B. Keimer, G. A. Sawatzky, and A. Damascelli, Symmetry of charge order in cuprates, Nature Mat. **14** (2015) 796.

[17] A. Yazdani, E. H. da Silva Neto, and P. Aynajian, Spectroscopic Imaging of Strongly Correlated Electronic States. Ann. Rev. Condens. Matt. Phys. **7** (2016) 11.

[18] D. W. Hess and J. W. Serene, Quasiparticle band structures and density-functional theory: single-particle excitations and band gaps in lattice models, Phys. Rev. B **59** (1999) 15617.

[19] R. Lopez-Sandoval and G. M. Pastor, Interaction-energy functional for lattice density functional theory: Application to one-, two-, and three-dimensional Hubbard models, Phys. Rev. B **69** (2004) 085101.

[20] D. D. Johnson, Modified Broyden's method for accelerating convergence in self-consistent calculations, Phys. Rev. B **38** (1988) 12807.